Engineered Iron-Oxide-Based Nanoparticles as Enhanced T_1 Contrast Agents for Efficient Tumor Imaging

Zijian Zhou,[†] Lirong Wang,[†] Xiaoqin Chi,[‡] Jianfeng Bao,[§] Lijiao Yang,[†] Wenxiu Zhao,[‡] Zhong Chen,[§] Xiaomin Wang,[‡] Xiaoyuan Chen,[∥] and Jinhao Gao[†,⊥,*]

[†]State Key Laboratory of Physical Chemistry of Solid Surfaces, The Key Laboratory for Chemical Biology of Fujian Province, and Department of Chemical Biology, College of Chemistry and Chemical Engineering, Xiamen University, Xiamen 361005, China, [‡]Xiamen Key Laboratory for Translational Medicine of Digestive Oncology, Research Institute of Digestive Disease, Zhongshan Hospital, Xiamen University, Xiamen 361004, China, [§]Department of Electronic Science and Fujian Key Laboratory of Plasma and Magnetic Resonance, Xiamen University, Xiamen 361005, China, [⊥]Center for Molecular Imaging and Translational Medicine, School of Public Health, Xiamen University, Xiamen 361005, China, and [∥]Laboratory of Molecular Imaging and Nanomedicine, National Institute of Biomedical Imaging and Bioengineering, National Institutes of Health, Bethesda, Maryland 20892, United States

ABSTRACT We report the design and synthesis of small-sized zwitterion-coated gadolinium-embedded iron oxide (GdIO) nanoparticles, which exhibit a strong T_1 contrast effect for tumor imaging through enhanced permeation and retention effect and the ability to clear out of the body in living subjects. The combination of spin-canting effects and the collection of gadolinium species within small-sized GdIO nanoparticles led to a significantly enhanced T_1 contrast effect. For example, GdIO nanoparticles with a diameter of ~4.8 nm exhibited a high r_1 relaxivity of 7.85 $mM^{-1} \cdot S^{-1}$ and a low r_2/r_1 ratio of 5.24. After being coated with zwitterionic dopamine sulfonate molecules, the 4.8 nm GdIO nanoparticles showed a steady hydrodynamic diameter (~5.2 nm) in both PBS buffer and fetal bovine serum solution, indicating a low nonspecific protein absorption. This study provides a valuable strategy for the design of highly sensitive iron-oxide-based T_1 contrast agents with relatively long circulation half-lives (~50 min), efficient tumor passive targeting (SKOV3, human ovarian cancer xenograft tumor as a model), and the possibility of rapid renal clearance after tumor imaging.

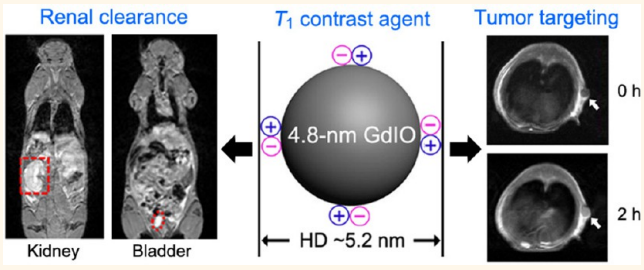

KEYWORDS: T_1 contrast agent · ultrasmall nanoparticle · zwitterionic · renal clearance · tumor imaging

The design and synthesis of various types of magnetic nanomaterials have attracted tremendous research interest in the areas of magnetic separation, drug delivery, and contrast agents for magnetic resonance imaging (MRI) in biomedical and clinical applications.[1−7] MRI is one of the most powerful noninvasive diagnosis techniques with superior resolution, permitting in-depth anatomical details in the diagnosis of many diseases.[8] Magnetic nanomaterials are employed as MRI contrast agents to improve the sensitivity and reliability because they are able to alter the relaxation time of nearby water protons to generate great contrast effects under external magnetic fields.[9,10] On the basis of the different models of longitudinal (T_1) and transverse (T_2) relaxations, there are two types of MRI contrast agents: positive (T_1) and negative (T_2). Generally speaking, superparamagnetic nanomaterials (*e.g.*, Fe_3O_4, $MnFe_2O_4$) are typically T_2 contrast materials,[11−13] and paramagnetic nanomaterials (*e.g.*, MnO, Gd_2O_3) are prevailing T_1 contrast materials.[14−16] Despite much progress in the development of T_1 contrast agents to minimize the toxicity issues of Mn^{2+} or Gd^{3+} by efficient metal chelation strategy,[17−20] they still suffer from poor biodistribution and potential release by demetalation or transmetalation with other ions such as Zn^{2+} in blood circulation, which results in increased risk of nephrogenic systemic fibrosis with renal dysfunction to patients.[21,22]

Ultrasmall (<3 nm) iron oxide (IO) nanoparticles are able to generate T_1 enhanced images owing to low magnetization by a strong surface spin-canting effect.[23−26] However, because of the high surface energy of such small particles, ultrasmall IO nanoparticles

* Address correspondence to jhgao@xmu.edu.cn.

Received for review December 26, 2012 and accepted March 8, 2013.

Published online March 08, 2013
10.1021/nn305991e

are likely to be rapidly dissolved and oxidized into Fe^{3+} ions in aqueous solution, leading to their instability in biological media. Therefore, IO-based nanoparticles with high stability and strong T_1 contrast effect are desirable as T_1 contrast agents. Normally, the spin-canted layer in IO nanoparticles is known to be 0.5−0.9 nm thick below the surface.[27,28] As depicted in Figure 1a, IO nanoparticles with a diameter of about 5 nm are considered to have a double-layer of core (spin-oriented)−shell (spin-canted) format. The spin-oriented core with high susceptibility would produce a high T_2 shortening effect, which may disturb and diminish the T_1 effect induced by the spin-canted shell. As a result, IO nanoparticles with a size larger than 5 nm usually show a strong T_2 contrast effect, while their T_1 effect was negligible. Herein, we introduce the novel small-sized (approximately 5 nm) gadolinium-embedded iron oxide (GdIO) nanoparticles as stable and improved T_1 contrast agents. The embedded Gd species can influence the long-range order of spins in iron oxide nanoparticles and induce an inner spin-canting effect, resulting in a fully spin-canted structure in GdIO nanoparticles (Figure 1b). Moreover, the collection of Gd species in GdIO nanoparticles (especially near the surface) may further lead to a great enhancement of T_1 contrast effects.[15]

For *in vivo* applications, nanoparticles are still struggling due to their metabolic fate and related toxicity issues, although we may control the interactions between nanoparticles and biological systems by tuning the properties of nanoparticles such as size, shape, and surface chemistry.[29−33] One would expect that nanoparticles with long circulation half-lives and the lowest likelihood of toxicity *in vivo* promise potential clinical translation.[34] The poor surface coating of nanoparticles usually suffers from a high uptake of macrophages and rapid accumulation in the mononuclear phagocyte system (MPS; *e.g.*, liver and spleen),[35] resulting in a short circulation half-life and long-term toxicity issues. The ideal surface coating of T_1 contrast nanomaterials should ensure an effective water-exchange ratio on the nearby surface of nanoparticles, a decrease in the nonspecific binding to plasma proteins in biological media, and an increase in the possibility of renal clearance.[36−38] Small zwitterion molecules may be the potential candidates to achieve such water-soluble nanoparticles by a ligand-exchange process.[39] The surface coating of nanoparticles using small zwitterion molecules as ligands may maintain the compact and small size of the nanoparticles, reduce nonspecific adsorption of proteins and interparticle agglomeration, increase the possibility of rapid renal clearance, lead to a potentially long circulation half-life *in vivo*,[40,41] and possibly deliver the host nanoparticles to leaky vascular tumors by a passive targeting strategy. We used the zwitterionic dopamine sulfonate (ZDS)[39] molecule as an effective binding ligand to modify the surface of small-sized GdIO nanoparticles (Figure 1c).

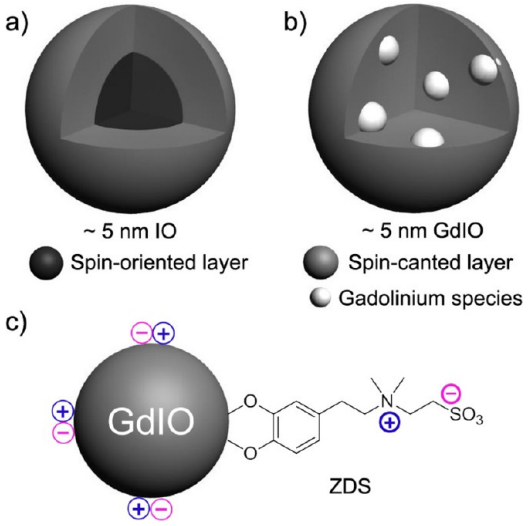

Figure 1. Schematic illustration of spin phenomena in small-sized (a) IO and (b) GdIO nanoparticles. The gadolinium species (Gd_2O_3 nanoclusters) in GdIO nanoparticles (~5 nm in diameter) cause an inner spin-canting effect, while the IO nanoparticles (~5 nm in diameter) contain a spin-canted surface and spin-oriented core. (c) Structure of GdIO nanoparticles coated with zwitterionic dopamine sulfonate (ZDS) molecules.

The ZDS-coated GdIO nanoparticles (GdIO@ZDS) showed a small hydrodynamic diameter (HD), low nonspecific binding to proteins, renal clearance, and most importantly, high passive tumor targeting for T_1 MRI imaging in living subjects.

RESULTS AND DISCUSSION

Preparation of Zwitterionic Small-Sized GdIO Nanoparticles. The synthesis of monodisperse GdIO nanoparticles with various small sizes is simple and straightforward: we employed iron(III) acetylacetonate and gadolinium(III) 2,4-pentanedionate hydrate as precursors to undergo a co-decomposition procedure in phenyl ether containing 1,2-hexadecanediol, oleyl amine, and oleic acid.[42] The sizes are easily tunable by reaction time without a size selection process. Particularly, GdIO nanoparticles with diameters of 2.8 ± 0.5, 3.5 ± 0.8, and 4.8 ± 0.6 nm were obtained in the reaction times of 20, 30, and 50 min, respectively. We also obtained monodisperse IO nanoparticles with a diameter of 4.9 ± 0.4 nm by similar procedures but without the Gd precursor for comparison. For simplicity, we used 2.8, 3.5, 4.8, and 4.9 nm to represent the average diameters of these nanoparticles (denoted as 2.8 nm GdIO, 3.5 nm GdIO, 4.8 nm GdIO, and 4.9 nm IO, respectively). The transmission electron microscopy (TEM) and high-resolution TEM (HRTEM) images showed that the as-synthesized GdIO and IO nanoparticles are nearly monodispersed with good crystallinity (Figure 2). The energy-dispersive X-ray spectroscopy (EDS) analysis and the XRD pattern of 4.8 nm GdIO nanoparticles indicated the presence of Gd_2O_3 nanoclusters (Figure S1). The electron spin resonance (ESR) spectra of 4.8 nm GdIO

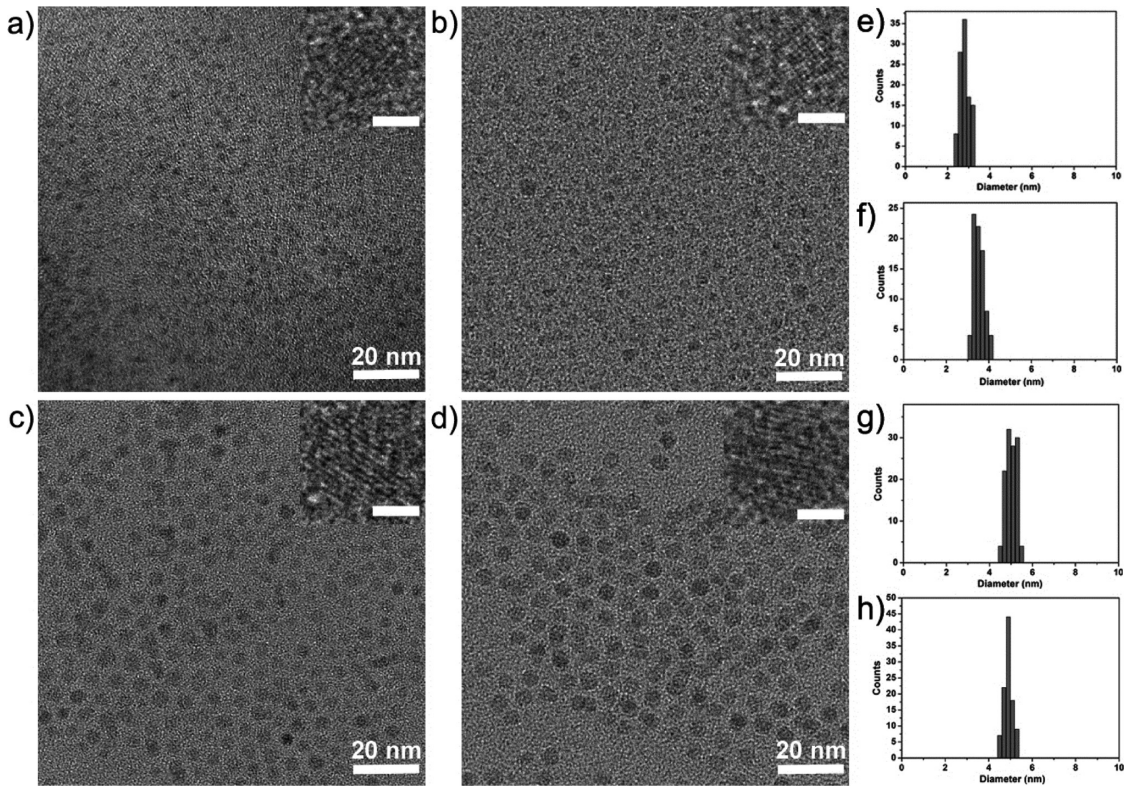

Figure 2. TEM images (insets: HRTEM images) and size distribution analysis of as-synthesized (a, e) 2.8 nm GdIO, (b, f) 3.5 nm GdIO, (c, g) 4.8 nm GdIO, and (d, h) 4.9 nm IO nanoparticles. Scale bar (insets): 2 nm.

nanoparticles showed an obvious decrease of ΔH_{pp} (from 928 to 689 G) and *g*-value (from 2.47 to 2.32) compared to those of 4.9 nm IO nanoparticles (Figure S2). This may be attributed to the weak magnetic moments for 4.8 nm GdIO nanoparticles caused by embedded Gd species.[43] Inductively coupled plasma atomic emission spectroscopy (ICP-AES) was used to quantify the percentages of embedded Gd^{3+} in all the samples. The results revealed that the Gd^{3+} percentage increased with the size of the GdIO nanoparticles (4.8 $\pm$ 1.1%, 6.5 $\pm$ 0.9%, and 7.2 $\pm$ 1.4% of Gd^{3+} in GdIO nanoparticles with diameters of 2.8, 3.5, and 4.8 nm, respectively).

We measured the magnetic properties of GdIO nanoparticles and 4.9 nm IO nanoparticles with a magnetic field of up to 5 T at temperatures of 300 K (Figure 3a) and 5 K (Figure 3b), respectively. The coercivity in hysteresis loops is negligible at 5 and 300 K in all the samples, while the magnetic moments tend to be unsaturated even at the maximal applied magnetic field of 5 T, indicating that these four samples exhibit partially paramagnetic behavior at room temperature. It is noteworthy that larger iron oxide nanoparticles (*e.g.*, 12 and 16 nm in diameter) showing obvious superparamagnetism at 300 K and ferromagnetism at 5 K were typical T_2 contrast agents.[25,44] Moreover, the much lower magnetic moment of 4.8 nm GdIO nanoparticles (~23 emu/g) than that of 4.9 nm IO nanoparticles (~36 emu/g) at 300 K is probably due to the lack of a spin-oriented layer, which further demonstrated that the gadolinium species is successfully embedded into the nanoparticles.[45] The embedded gadolinium species (*e.g.*, Gd_2O_3 nanoclusters) may disturb the long-range order of magnetic spins in iron oxide nanoparticles. Together with the surface-canting effect, the magnetic spins in the 4.8 nm GdIO nanoparticles are proposed to be fully canted, resulting in a relatively low magnetic moment. In the case of the 2.8 nm GdIO nanoparticles, the great increment of magnetic moments from 300 to 5 K may be attributed to the relative instability due to the strong spin-canting effect.

To achieve water-soluble nanoparticles, we introduced a simple method to prepare ZDS or *meso*-2,3-dimercaptosuccinic acid (DMSA)[46] solely coated nanoparticles through an inhomogeneous phase transfer process. Briefly, ZDS molecules in water and the nanoparticles in hexane were mixed to form a double-layer system, which then underwent a ligand-exchange process. Because the chelation capability of the dopamine moiety to the IO surface is much stronger than that of the original carboxyl or amine groups, the nanoparticles were gradually transferred into water by replacing oleic acid or oleyl amine with ZDS molecules. DMSA-coated nanoparticles were obtained with similar procedures. Finally, the aqueous samples were stored at 4 °C for further use.

Relaxivity Measurements. We performed the relaxivity test and magnetic resonance imaging on a 7 T MRI scanner. The GdIO nanoparticles with the sizes 2.8, 3.5, and 4.8 nm showed r_1 values of 3.09 $\pm$ 0.12, 4.63 $\pm$ 0.08, and 7.85 $\pm$ 0.11 $mM^{-1}\cdot S^{-1}$ (Fe + Gd), respectively

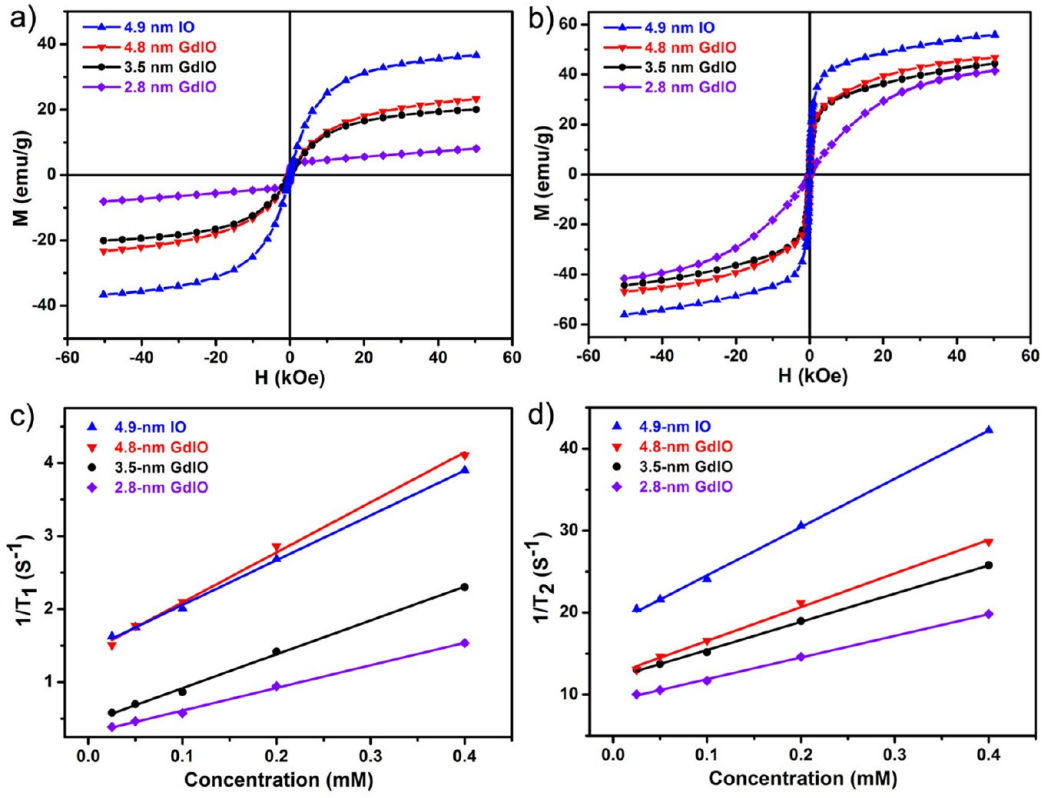

e)

	r_1 ($mM^{-1}S^{-1}$)	r_2 ($mM^{-1}S^{-1}$)	r_2/r_1
4.8-nm GdIO	7.85	41.14	5.24
3.5-nm GdIO	4.63	34.38	7.43
2.8-nm GdIO	3.05	26.45	8.56
4.9-nm IO	6.14	58.94	9.59

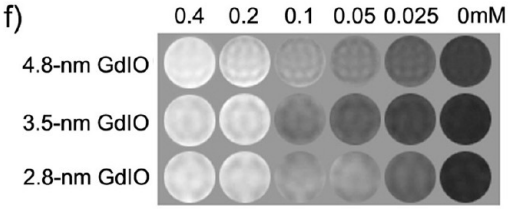

Figure 3. Magnetic properties and MRI measurements of 4.9 nm IO, 4.8 nm GdIO, 3.5 nm GdIO, and 2.8 nm GdIO nanoparticles. Field-dependent magnetization curves ($M-H$) at (a) 300 K and (b) 5 K, respectively. Plots of (c) $1/T_1$ and (d) $1/T_2$ against concentrations of total metal ions (Fe + Gd). (e) Comparison of r_1 and r_2 values obtained from the slopes in (c) and (d), together with the r_2/r_1 values. (f) T_1 phantom images of 4.8, 3.5, and 2.8 nm GdIO nanoparticles with different concentrations of total metal ions (Fe + Gd).

(Figure 3c and e), suggesting that 4.8 nm GdIO nanoparticles may have a strong T_1 contrast effect. However, the r_1 value of 4.9 nm IO nanoparticles dropped to 6.14 $\pm$ 0.22 $mM^{-1}\cdot S^{-1}$. It is known that gadolinium species possessing seven unpaired electrons are excellent candidates as T_1 contrast materials. The commercial contrast agent Gd-DTPA revealed a moderate r_1 value of 3.30 $\pm$ 0.25 $mM^{-1}\cdot S^{-1}$ under the same measured conditions (Figure S3), indicating that 4.8 nm GdIO nanoparticles may have better T_1 contrast efficacy than Gd-DTPA. It should be noted that the dose of Gd in Gd-DTPA is about 30-fold higher than that in 4.8 nm GdIO nanoparticles to achieve comparable T_1 signal enhancement. The Gd_2O_3 nanoclusters in GdIO nanoparticles extended the spin-canting effect by perturbation of long-range order magnetic spins in iron oxide nanoparticles. As expected, the higher r_1 value of 4.8 nm GdIO nanoparticles compared to that of 4.9 nm IO nanoparticles is probably due to the enhanced T_1 shortening effect by the collection of Gd^{3+} ions (especially close to the surface of nanoparticles) and enhanced spin-canting effect by embedding Gd species in GdIO nanoparticles.[45] The r_2 values of magnetic nanoparticles are highly dependent on their magnetic susceptibility under external magnetic fields.[9,11] The GdIO nanoparticles with a strong spin-canting effect exhibited low magnetic moments, leading to a weak T_2 contrast efficacy, whereas the 4.9 nm IO nanoparticles possessing the largest magnetic moment showed the highest r_2 value among these four samples under the same experimental conditions (Figure 3d and e). It is noteworthy that both paramagnetic and superparamagnetic nanomaterials have T_1 and T_2 shortening effects, while the r_2/r_1 ratio is a key factor to evaluate the potentially preferable T_1 or T_2 contrast efficacy for a given material.[25] That is, the contrast agents with lower r_2/r_1 ratio would show a stronger T_1 effect. The 4.8 nm GdIO nanoparticles had a remarkably low r_2/r_1 value of 5.24 $\pm$ 0.18 (Figure 3e), suggesting that 4.8 nm GdIO nanoparticles are more efficient T_1 contrast agents than 2.8 nm and 3.5 nm GdIO nanoparticles (r_2/r_1 ratios

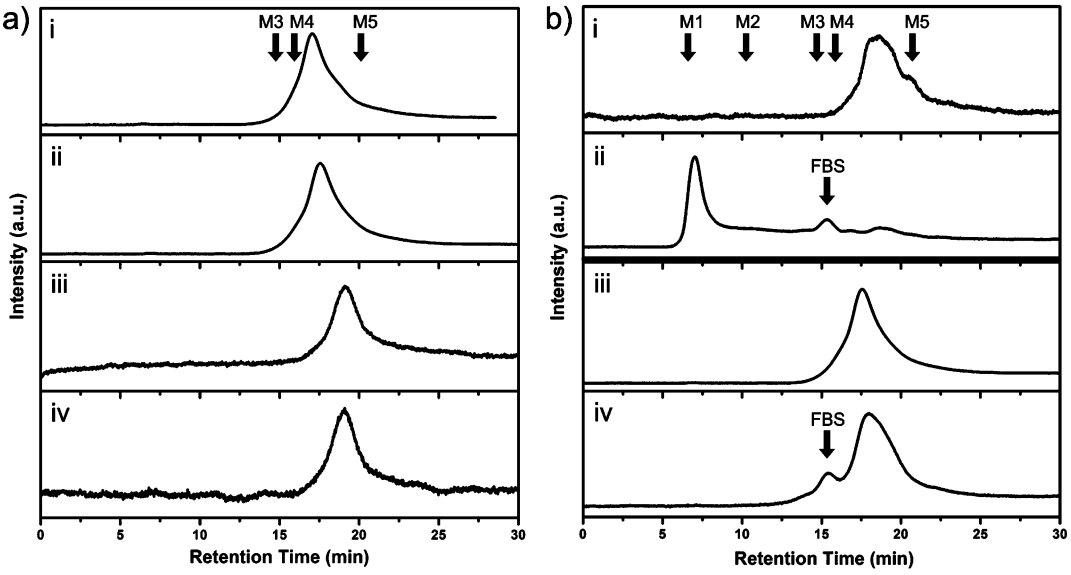

Figure 4. Gel-filtration chromatography (GFC) profiles and size analysis of various nanoparticles in PBS buffer and FBS solution. Note that the sizes of nanoparticles are inversely related to the retention times. (a) i–iv show the chromatograms of 4.9 nm IO@ZDS, 4.8 nm GdIO@ZDS, 3.5 nm GdIO@ZDS, and 2.8 nm GdIO@ZDS in PBS buffer (the absorbance of 365 nm), respectively. (b) Comparison of chromatograms of (i, ii) 4.8 nm GdIO@DMSA and (iii, iv) 4.8 nm GdIO@ZDS in (i, iii) PBS buffer and (ii, iv) 20% FBS solution (after 4 h incubation), respectively. Arrows in (ii) and (iv) indicate the retention time of FBS. Protein markers M1 (blue dextran, 29.5 nm HD), M2 (thyroglobulin, 18.8 nm HD), M3 (alcohol dehydrogenase, 10.1 nm HD), M4 (ovalbumin, 6.1 nm HD), and M5 (vitamin B_{12}, 1.5 nm HD) are shown by arrows.

are 8.56 and 7.43, respectively). These results are comparable to 3 nm sized iron oxide nanoparticles with an r_2/r_1 value of 6.12 with a 3 T MRI scanner reported previously.[25] The T_1 MRI phantom study revealed that all of the small-sized GdIO nanoparticles exhibited T_1 contrast enhancement (Figure 3f). However, the 4.9 nm IO nanoparticles showed a T_2 contrast effect but no obvious T_1 contrast effect (Figure S3) because of the relatively high r_2/r_1 ratio of 9.59 $\pm$ 0.24 ($p < 0.05$ significantly different compared to the r_2/r_1 value of 4.8 nm GdIO nanoparticles). However, the coating molecules ZDS alone did not show any detectable T_1 contrast effect (Figure S3).

***In Vitro* and *in Vivo* Behavior Studies.** To investigate the size changes of ZDS- or DMSA-coated GdIO nanoparticles in a biological solution, we used gel filtration chromatography (GFC) to determine the hydrodynamic diameters (HDs) of nanoparticles in biological media because this system allows online and full-spectrum analysis with high reliability and repeatability. The GFC profiles indicated the sizes of nanoparticles are inversely related to the retention times. We first tested a group of protein standards as markers to calibrate the HDs, for example, blue dextran (M1, 6.9 min, 29.5 nm HD), thyroglobulin (M2, 10.9 min, 18.8 nm HD), alcohol dehydrogenase (M3, 14.8 min, 10.1 nm HD), ovalbumin (M4, 16.0 min, 6.1 nm HD), and vitamin B_{12} (M5, 20.5 min, 1.5 nm HD). Under the same conditions, the various ZDS-coated nanoparticles with different sizes were nearly monodisperse with sharp peaks of retention time (Figure 4a, i–iv). These results showed that the HDs of ZDS-coated samples were in the range from 1.5 to 6.1 nm (*e.g.*, the HD of 4.8 nm GdIO@ZDS nanoparticles is approximately 5.2 nm), indicating the extremely thin surface coating layer (<1 nm) on the nanoparticles. The dynamic light scattering (DLS) results showed comparable HDs of about 4.18, 5.61, 6.50, and 7.13 nm for 2.8, 3.5, and 4.8 nm GdIO@ZDS and 4.9 nm IO@ZDS nanoparticles, respectively (Figure S4), which is consistent with the GFC analysis.

We then studied the GFC profiles of GdIO@ZDS and GdIO@DMSA in PBS buffer or serum solution. Using 4.8 nm GdIO nanoparticles as an example, the GFC results showed that GdIO@DMSA nanoparticles have a nearly monodisperse characteristic in PBS buffer with an HD smaller than 6.1 nm (Figure 4b, i). However, we observed a strong peak appeared at 6.9 min while the peak at ~18 min disappeared after incubation with 20% fetal bovine serum (FBS) for 4 h (Figure 4b, ii), indicating that the growth of the HD of GdIO@DMSA to about 29 nm because of the serious nonspecific binding of the nanoparticles to serum proteins and further aggregation of nanoparticles during the incubation. On the contrary, GdIO@ZDS showed a steady retention time in both PBS buffer and FBS solution (Figure 4b, iii and iv) because the zwitterionic nanoparticles tend to avoid nonspecific adsorption of serum proteins. The small peak at the retention time of 15.3 min suggested the existence of residual FBS (Figure 4b, ii), which was further confirmed by the control experiment (Figure S5). The TEM images also indicated the good colloidal monodispersity of 4.8 nm GdIO@ZDS nanoparticles in both PBS buffer and serum solutions after 4 h incubation (Figure S6). After the nonspecific adsorption of serum proteins, GdIO@DMSA nanoparticles would be easily recognized by macrophages

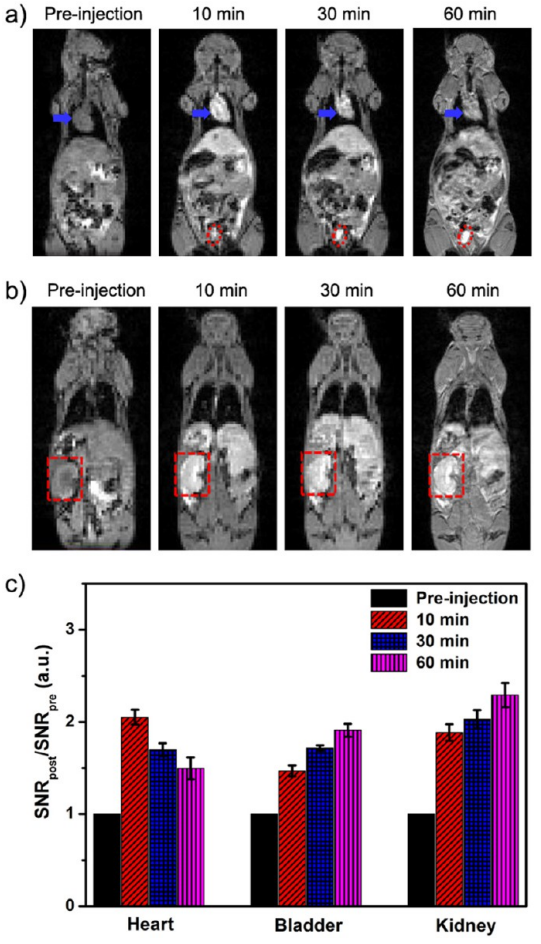

Figure 5. *In vivo* T_1 **MR imaging and analysis of mice after intravenous injection of 4.8 nm GdIO@ZDS nanoparticles as contrast agents. (a, b) MR images of mice after tail vein injection of 4.8 nm GdIO@ZDS nanoparticles (2.0 mg/kg) at 0, 10, 30, and 60 min, respectively. Blue arrows, heart; red dot circles, bladder; red dashed squares, kidney. (c) Quantification of signal changes (SNR ratio) in heart, bladder, and kidney at different time points after administration (*n* = 3).**

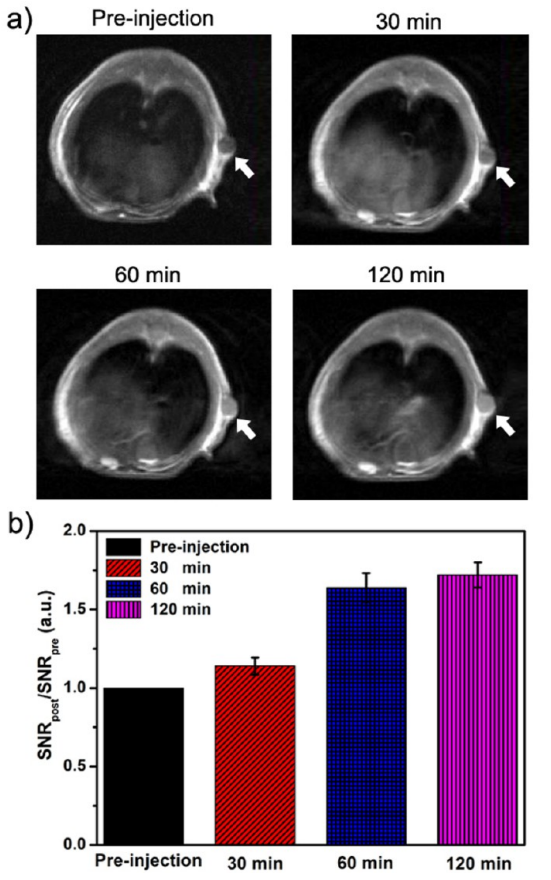

Figure 6. T_1 **MR imaging and quantificational analysis of SKOV3 human ovarian cancer xenograft tumors after intravenous injection of 4.8 nm GdIO@ZDS nanoparticles. (a)** T_1**-weighted MR images of nude mice bearing subcutaneous tumors (white arrows) after intravenous injection of GdIO@ZDS nanoparticles (2.0 mg/kg) at 30, 60, and 120 min, respectively. The MR image before injection was acquired for comparison. (b) Quantificational analysis of signal changes (SNR ratio) in tumors at different time points after administration (*n* = 3).**

and accumulate in tissues in the MPS, *e.g.*, liver and spleen. As a result, the hepatobiliary system will be a major clearance route to degrade GdIO@DMSA nanoparticles into metal ions in the bile, which leads to an increased risk of toxicity. Another serious problem is that the retention of metal ions at a high dose in the body may interfere with other radiological tests, for example, CT imaging.[41] The 4.8 nm GdIO@ZDS nanoparticles showed a very small HD of about 5.2 nm in both PBS buffer and serum, which ensures that the zwitterionic GdIO@ZDS nanoparticles meet the requirement of the size threshold for renal clearance.[41] Considering the potential toxicity of heavy metals, the systemic toxicity study (*e.g.*, brain toxicity and kidney damage)[47−49] of GdIO nanoparticles to living subjects should be conducted in the future; the rapid renal clearance of nanoparticles could significantly minimize the long-term toxicity issues in the body. Moreover, small-sized nanoparticles circulating in the blood may also increase the possibility of passive targeting in tumors by the enhanced permeation and retention (EPR) effect.

Because of the significantly different behaviors between GdIO@ZDS and GdIO@DMSA in serum, we investigated their circulation fate *in vivo* with a 7 T MRI scanner using BALB/c mouse as a model. After intravenous injection of 4.8 nm GdIO@ZDS at a dose of 2.0 mg/kg (with respect to the weight of Fe_3O_4 and Gd_2O_3 constituents compared with the mouse body weight), T_1 MR images were then acquired at the time points of 10, 30, and 60 min, respectively. We observed a great contrast enhancement in the heart, kidneys, and bladder at 10 min postinjection (p.i., Figure 5a and b). The signal in the heart slightly decreased over time, while the signals in the kidneys and bladder increased over time. To quantify the contrast, we calculated the signal-to-noise ratio (SNR) by finely analyzing regions of interest (ROIs) of the MR images and calculated the values of SNR_{post}/SNR_{pre} to represent the signal changes (Figure 5c). The SNR values were calculated according to $SNR_{ROIs} = SI_{ROIs}/SD_{noise}$ (SI stands for signal intensity and SD stands for standard deviation).[50] The signal changes in the heart region were 2.05 ± 0.04, 1.69 ± 0.07, and 1.5 ± 0.09

at 10, 30, and 60 min p.i., respectively, indicating the slow elimination of contrast agent from blood during circulation. We estimated the half-life of GdIO@ZDS to be about 50 min in mice (Figure S7), which is much longer than that of Gd complex small molecules, with a high excretion rate (half-life of about several minutes in small animals).[51] Moreover, the bladder and kidneys displayed significantly increased signal changes, strongly suggesting renal excretion of the GdIO@ZDS nanoparticles. We further confirmed the existence of Gd (4.09 ± 1.07 μg/mL) and Fe ions (52.45 ± 0.88 μg/mL) in urine (collected at 4 h p.i.) by inductively coupled plasma mass spectroscopy (ICP-MS). Renal clearance requires the final HDs of nanoparticles of less than approximately 6 nm to undergo glomerular filtration, tubular filtration, and finally urinary excretion processes.[36] These results indicated that the zwitterionic coating plays an important role in optimizing the *in vivo* behaviors of nanoparticles, which will likely cause very low risk of toxicity associated with long retention and cellular catabolism in the body.

We also acquired T_1 MR images of mice injected with 4.8 nm GdIO@DMSA nanoparticles (Figures S8 and S9). Unlike the case of GdIO@ZDS, the mouse liver exhibited obvious T_1 signal changes after intravenous injection of GdIO@DMSA nanoparticles, indicating the high accumulation of GdIO@DMSA nanoparticles in the liver. However, the kidneys did not show any signal change over time. GdIO@DMSA nanoparticles with negative surface charge had obvious nonspecific adsorption of serum proteins in the blood, which led to recognition by the immunologic system and capture by the MPS (*e.g.*, liver, spleen, and lymph nodes) through endocytosis.[50,52,53] The high uptake of nanoparticles by the MPS can dramatically decrease the blood circulation time and increase the retention time in normal tissues (*e.g.*, slow hepatic clearance), which may cause potential long-term toxicity to the living subjects. To further validate the biodistribution of GdIO@ZDS and GdIO@DMSA nanoparticles in mice, we performed Prussian blue staining of sections of the major organs from mice injected with the two nanoparticles (Figure S10). Both the GdIO@ZDS and GdIO@DMSA nanoparticles had visible blue spots in the spleen and liver (GdIO@DMSA nanoparticles had a much brighter staining signal in the liver than GdIO@ZDS nanoparticles), while only GdIO@ZDS nanoparticles showed positive staining in the kidneys and heart.

Passive Tumor Targeting and T_1 Imaging. GdIO@ZDS nanoparticles with a strong T_1 contrast effect and small HD may provide great opportunity for imaging tumors through the EPR effect. We thus established a subcutaneous SKOV3 ovarian cancer model to evaluate the passive targeting ability of 4.8 nm GdIO@ZDS nanoparticles using MRI. The efficiency of passive targeting through leaky vasculature of a tumor is highly dependent on the blood circulation half-life: the longer the half-life, the higher the tumor uptake. After intravenous injection of 4.8 nm GdIO@ZDS nanoparticles (2.0 mg/kg), we observed the increase of T_1 contrast in the tumor over time and remarkable T_1 contrast from the surrounding normal tissue at 2 h p.i. (Figure 6a). The signal changes in the tumor were 1.14 ± 0.05, 1.64 ± 0.09, and 1.72 ± 0.08 at 30, 60, and 120 min p.i., respectively (Figure 6b). The slowly increasing signal changes over time indicated the effective uptake of contrast agents in the tumor through the EPR effect. Taking advantage of nanoparticle-based probes with relatively long blood half-life, the GdIO nanoparticles were more likely to leak into tumors through the EPR effect compared with the molecular-based contrast agents (*e.g.*, Gd-DTPA). Because of the rapid renal clearance of 4.8 nm GdIO nanoparticles, we noticed that the signal changes in the tumor dropped after 4 h p.i. (Figure S11). It is necessary to conduct MR scanning within 2−4 h after administration of 4.8 nm GdIO nanoparticles, which also meets the basic requirements of clinical diagnosis. The contrast agents should be cleared out of the body as soon as possible after their performance in disease diagnosis so that there is a low chance of toxicity, which endows them with great potential for further clinical translation.[19,54,55]

CONCLUSION

In summary, we have demonstrated that small-sized GdIO nanoparticles are excellent T_1 contrast agents in both *in vitro* and *in vivo* studies because of the collection of gadolinium species and the enhanced inner spin-canting within the nanoparticles. This Gd-embedding strategy may open new avenues in the design of iron-oxide-based nanomaterials with strong T_1 contrast enhancement. The zwitterionic dopamine sulfonate (ZDS)-coated 4.8 nm GdIO nanoparticles with small hydrodynamic diameter (~5.2 nm) and minimal nonspecific binding to serum proteins in living subjects led to a relatively long circulation half-life, efficient renal clearance, and EPR effect-based tumor contrast. The desirable features of small-sized GdIO@ZDS nanoparticles make these engineered iron-oxide-based nanomaterials suitable candidates as excellent T_1 contrast agents for tumor imaging and disease diagnosis.

MATERIALS AND METHODS

Materials. Oleylamine (tech 70%), oleic acid (tech 90%), phenyl ether (99%), 1,2-hexadecanediol (98%), 3-hydroxytyramine hydrochloride, and iron(III) acetylacetonate (99%) were purchased from Acros; gadolinium(III) 2,4-pentanedionate hydrate (99.9%), 1,3-propanesultone (99%), and *meso*-2,3-dimercaptosuccinic acid were purchased from Alfa Aesar. Other reagents were purchased from Sinopharm Chemical Reagent Co. Ltd. The Superose-6 10/300 GL column was purchased from GE Healthcare Life Sciences. All chemicals were used as received without further purification.

Characterization. TEM and HRTEM images were recorded on a JEM-2100 microscope at an accelerating voltage of 200 kV. The hysteresis loop (at 300 and 5 K) was recorded on a Quantum Design MPMS-XL-7 system. The element analysis of Fe and Gd in the samples was measured by inductively coupled plasma atomic emission spectroscopy (ICP-AES) or inductively coupled plasma mass spectroscopy (ICP-MS). The ESR spectra were recorded on an ESR spectrometer (Bruker ESR spectrometer EMX-10/12) at 90 K. The dynamic light scattering measurements were performed on a Malvern Zetasizer Nano ZS instrument. The MRI measurements and T_2/T_1 relaxation time testing were performed on a 7 T MRI scanner (Varian 7 T Micro MRI System). Gel-filtration chromatography analysis was performed on a Superose-6 10/300 GL column (GE Healthcare Life Sciences) on an HPLC system (UltiMate 3000, DIONEX).

Synthesis of Small-Sized GdIO and IO Nanoparticles. GdIO nanoparticles with various sizes were synthesized through thermal decomposition of iron(III) acetylacetonate and gadolinium(III) 2,4-pentanedionate with different reaction times. Briefly, iron-(III) acetylacetonate (353 mg, 1 mmol), gadolinium(III) 2,4-pentanedionate hydrate (54 mg, 0.1 mmol), oleyl amine (0.6 mL), oleic acid (0.6 mL), and 1,2-hexadecanediol (410 mg) were mixed in a three-neck bottle flask containing phenyl ether (15 mL). The solution was heated to reflux temperature with a heating rate of 5 °C min^{-1} under an inert atmosphere. The 2.8, 3.5, and 4.8 nm GdIO nanoparticles were obatained by ceasing heating at 20, 30, and 50 min after reaching reflux point, respectively. After cooling to room temperature, excess ethanol was added to precipitate the nanoparticles. The product was collected by centrifugation and finally redispersed in hexane. The synthesis of 4.9 nm IO nanoparticles was similar to the synthesis of 4.8 nm GdIO nanoparticles but without gadolinium precursor. All samples were stored at 4 °C for further use.

Preparation of ZDS- and DMSA-Coated Nanoparticles. The preparation of ZDS- or DMSA-coated nanoparticles was carried out through a ligand-exchange process. For example, ZDS (10 mg) was dissolved in 10 mL of water in a three-neck flask, and the system was degassed with N_2. The as-prepared 4.8 nm GdIO nanoparticles (100 μmol) dissolved in hexane were added to the flask. The solution was then heated to reflux for 2 h before cooling to room temperature. The nanoparticles were obtained in the bottom layer, suggesting the successful ZDS coating. DMSA-coated nanoparticles were prepared by changing ZDS to DMSA in a similar manner. The obtained water-soluble nanoparticles were further purified with a NAP-10 column and stored at 4 °C.

Gel Filtration Chromatography. We performed the GFC analysis on a Superose-6 10/300 GL column (GE Healthcare Life Sciences) by high-performance liquid chromatography (HPLC) (UltiMate 3000, Dionex) monitored at the absorbance of 365 nm, using PBS buffer (1×, pH 7.4) as the mobile phase. The flow rate was 1.0 mL/min. The calibration of hydrodynamic diameter was performed by injecting 100 μL of protein standards containing blue dextran (2000 kDa, 29.5 nm HD), thyroglobulin (669 kDa, 18.0 nm HD), alcohol dehydrogenase (150 kDa, 10.1 nm HD), ovalbumin (44 kDa, 6.13 nm HD), and vitamin B_{12} (1.35 kDa, 1.5 nm HD), denoted as M1−M5 sequentially. For the serum binding test, 1 μM nanoparticles were mixed with 20% FBS solution and incubated for 4 h at 37 °C before running a GFC column. All standards and samples were tested in triplicate.

MRI Phantom Study. The samples for MRI phantom study were prepared separately. Each type of nanoparticle was prepared with concentrations of 400, 200, 100, 50, and 25 μM of total metal ions (Fe + Gd) in 1% agar-containing solution. The control sample denoted as 0 μM was prepared with purified water containing 1% agar. The longitudinal and transverse relaxation times were measured (at 298 K) and used for calculating the relaxation rate of the samples. T_2-weighted and T_1-weighted MR images of all the samples were acquired under the following parameters: TR/TE = 3000/60 ms (T_2), TR/TE = 300/12 ms (T_1), 256 × 256 matrices, repetition times = 4.

***In Vivo* MRI Study.** Animal experiments were executed according to the protocol approved by Institutional Animal Care and Use Committee of Xiamen University. Before *in vivo* experiments, the GdIO@ZDS and GdIO@DMSA samples were filtered through sterilized membrane filters (pore size 0.22 μm) and stored in sterilized vials for further use. For *in vivo* MRI studies, the transverse images of BALB/c mice were first acquired at different slices to show the heart, kidneys, and bladder planes. The mice were then intravenously injected with 100 μL of 4.8 nm GdIO@ZDS solution (2.0 mg/kg). Time-scale acquisition of postinjection images at 10, 30, and 60 min were obtained with the same slices. The T_1 MR images of mice injected with 4.8 nm GdIO@DMSA solution were acquired in a similar manner. The acquisition process contained transverse and coronal planes at the postinjection time points of 1, 2, and 4 h. All the images were acquired using fSEMS sequence under the following parameters: TR/TE = 300/10 ms, 256 × 256 matrices, slices = 5, thickness = 2 mm, averages = 2, FOV = 80 × 80.

Tumor Imaging. The subcutaneous tumor model was established on four-week-old nude mice. Suspended SKOV3 cancer cells (50 μL) at a density of 1×10^7 cells per milliliter were injected subcutaneously into the right front flanks. After 3−4 weeks, the tumor-bearing mice were injected with 4.8 nm GdIO@ZDS nanoparticles (2.0 mg/kg) *via* tail vein. The coronal plane images across the tumor were acquired at time points of 15, 30, 60, 120, and 240 min postinjection. The images were acquired under the following parameters: TR/TE = 400/10 ms, 256 × 256 matrices, slices = 3, thickness = 2 mm, averages = 4, FOV = 60 × 60.

Conflict of Interest: The authors declare no competing financial interest.

Acknowledgment. This work was partially supported by the National Key Basic Research Program of China (2013CB933901 and 2013CB733802), National Natural Science Foundation of China (21021061, 21222106, 81000662, and 81201805), and Program for New Century Excellent Talents in University (NCET-10-0709).

Supporting Information Available: The experimental section, EDS analysis, ESR spectra, DLS measurements, XRD patterns, MR phantom images, GFC profile, half-life study, *in vivo* MRI study, Prussian blue staining, and MR images of tumors. This material is available free of charge *via* the Internet at http://pubs.acs.org.

REFERENCES AND NOTES

1. McCarthy, J. R.; Weissleder, R. Multifunctional Magnetic Nanoparticles for Targeted Imaging and Therapy. *Adv. Drug Delivery Rev.* **2008**, *60*, 1241–1251.
2. Sun, C.; Lee, J. S. H.; Zhang, M. Magnetic Nanoparticles in MR Imaging and Drug Delivery. *Adv. Drug Delivery Rev.* **2008**, *60*, 1252–1265.
3. Hu, F.; Joshi, H. M.; Dravid, V. P.; Meade, T. J. High-Performance Nanostructured MR Contrast Probes. *Nanoscale* **2010**, *2*, 1884.
4. Colombo, M.; Carregal-Romero, S.; Casula, M. F.; Gutierrez, L.; Morales, M. P.; Bohm, I. B.; Heverhagen, J. T.; Prosperi, D.; Parak, W. J. Biological Applications of Magnetic Nanoparticles. *Chem. Soc. Rev.* **2012**, *41*, 4306–4334.
5. Cheon, J.; Lee, J. H. Synergistically Integrated Nanoparticles as Multimodal Probes for Nanobiotechnology. *Acc. Chem. Res.* **2008**, *41*, 1630–1640.
6. Gao, J. H.; Gu, H. W.; Xu, B. Multifunctional Magnetic Nanoparticles: Design, Synthesis, and Biomedical Applications. *Acc. Chem. Res.* **2009**, *42*, 1097–1107.
7. Reddy, L. H.; Arias, J. L.; Nicolas, J.; Couvreur, P. Magnetic Nanoparticles: Design and Characterization, Toxicity and Biocompatibility, Pharmaceutical and Biomedical Applications. *Chem. Rev.* **2012**, *112*, 5818–5878.
8. Liang, Z. P.; Lauterbur, P. C. *Principles of Magnetic Resonance Imaging: A Signal Processing Perspective*; Wiley-IEEE Press, 1999.
9. Na, H. B.; Song, I. C.; Hyeon, T. Inorganic Nanoparticles for MRI Contrast Agents. *Adv. Mater.* **2009**, *21*, 2133–2148.
10. Schladt, T. D.; Schneider, K.; Schild, H.; Tremel, W. Synthesis and Bio-Functionalization of Magnetic Nanoparticles for Medical Diagnosis and Treatment. *Dalton Trans.* **2011**, *40*, 6315–6343.

11. Lee, J.-H.; Huh, Y.-M.; Jun, Y.-w.; Seo, J.-w.; Jang, J.-t.; Song, H.-T.; Kim, S.; Cho, E.-J.; Yoon, H.-G.; Suh, J.-S.; *et al*. Artificially Engineered Magnetic Nanoparticles for Ultra-Sensitive Molecular Imaging. *Nat. Med.* **2006**, *13*, 95–99.
12. Cheong, S.; Ferguson, P.; Feindel, K. W.; Hermans, I. F.; Callaghan, P. T.; Meyer, C.; Slocombe, A.; Su, C.-H.; Cheng, F.-Y.; Yeh, C.-S.; *et al*. Simple Synthesis and Functionalization of Iron Nanoparticles for Magnetic Resonance Imaging. *Angew. Chem., Int. Ed.* **2011**, *50*, 4206–4209.
13. Tassa, C.; Shaw, S. Y.; Weissleder, R. Dextran-Coated Iron Oxide Nanoparticles: A Versatile Platform for Targeted Molecular Imaging, Molecular Diagnostics, and Therapy. *Acc. Chem. Res.* **2011**, *44*, 842–852.
14. Na, H. B.; Lee, J. H.; An, K.; Park, Y. I.; Park, M.; Lee, I. S.; Nam, D.-H.; Kim, S. T.; Kim, S.-H.; Kim, S.-W.; *et al*. Development of a T_1 Contrast Agent for Magnetic Resonance Imaging Using MnO Nanoparticles. *Angew. Chem., Int. Ed.* **2007**, *46*, 5397–5401.
15. Park, J. Y.; Baek, M. J.; Choi, E. S.; Woo, S.; Kim, J. H.; Kim, T. J.; Jung, J. C.; Chae, K. S.; Chang, Y.; Lee, G. H. Paramagnetic Ultrasmall Gadolinium Oxide Nanoparticles as Advanced T_1 MRI Contrast Agent: Account for Large Longitudinal Relaxivity, Optimal Particle Diameter, and *in Vivo* T_1 MR Images. *ACS Nano* **2009**, *3*, 3663–3669.
16. Mahajan, S. V.; Dickerson, J. H. Synthesis of Monodisperse Sub-3 nm RE_2O_3 and Gd_2O_3: RE^{3+} Nanocrystals. *Nanotechnology* **2007**, *18*, 325605.
17. Caravan, P.; Ellison, J. J.; McMurry, T. J.; Lauffer, R. B. Gadolinium(III) Chelates as MRI Contrast Agents: Structure, Dynamics, And Applications. *Chem. Rev.* **1999**, *99*, 2293–2352.
18. Kobayashi, H.; Longmire, M. R.; Ogawa, M.; Choyke, P. L. Rational Chemical Design of the Next Generation of Molecular Imaging Probes Based on Physics and Biology: Mixing Modalities, Colors and Signals. *Chem. Soc. Rev.* **2011**, *40*, 4626–4648.
19. Cole, A. J.; Yang, V. C.; David, A. E. Cancer Theranostics: The Rise of Targeted Magnetic Nanoparticles. *Trends Biotechnol.* **2011**, *29*, 323–332.
20. Caravan, P. Protein-Targeted Gadolinium-Based Magnetic Resonance Imaging (MRI) Contrast Agents: Design and Mechanism of Action. *Acc. Chem. Res.* **2009**, *42*, 851–862.
21. High, W. A.; Ayers, R. A.; Chandler, J.; Zito, G.; Cowper, S. E. Gadolinium is Detectable within the Tissue of Patients with Nephrogenic Systemic Fibrosis. *J. Am. Acad. Dermatol.* **2007**, *56*, 21–26.
22. Marckmann, P.; Skov, L.; Rossen, K.; Dupont, A.; Damholt, M. B.; Heaf, J. G.; Thomsen, H. S. Nephrogenic Systemic Fibrosis: Suspected Causative Role of Gadodiamide Used for Contrast-Enhanced Magnetic Resonance Imaging. *J. Am. Soc. Nephrol.* **2006**, *17*, 2359–2362.
23. Tromsdorf, U. I.; Bruns, O. T.; Salmen, S. C.; Beisiegel, U.; Weller, H. A Highly Effective, Nontoxic T_1 MR Contrast Agent Based on Ultrasmall PEGylated Iron Oxide Nanoparticles. *Nano Lett.* **2009**, *9*, 4434–4440.
24. Neuwelt, E. A.; Hamilton, B. E.; Varallyay, C. G.; Rooney, W. R.; Edelman, R. D.; Jacobs, P. M.; Watnick, S. G. Ultrasmall Superparamagnetic Iron Oxides (USPIOs): A Future Alternative Magnetic Resonance (MR) Contrast Agent for Patients at Risk for Nephrogenic Systemic Fibrosis (NSF)? *Kidney Int.* **2008**, *75*, 465–474.
25. Kim, B. H.; Lee, N.; Kim, H.; An, K.; Park, Y. I.; Choi, Y.; Shin, K.; Lee, Y.; Kwon, S. G.; Na, H. B.; *et al*. Large-Scale Synthesis of Uniform and Extremely Small-Sized Iron Oxide Nanoparticles for High-Resolution T_1 Magnetic Resonance Imaging Contrast Agents. *J. Am. Chem. Soc.* **2011**, *133*, 12624–12631.
26. Taboada, E.; Rodríguez, E.; Roig, A.; Oró, J.; Roch, A.; Muller, R. N. Relaxometric and Magnetic Characterization of Ultrasmall Iron Oxide Nanoparticles with High Magnetization. Evaluation as Potential T_1 Magnetic Resonance Imaging Contrast Agents for Molecular Imaging. *Langmuir* **2007**, *23*, 4583–4588.
27. Coey, J. M. D. Noncollinear Spin Arrangement in Ultrafine Ferrimagnetic Crystallites. *Phys. Rev. Lett.* **1971**, *27*, 1140–1142.
28. Linderoth, S.; Hendriksen, P. V.; Bodker, F.; Wells, S.; Davies, K.; Charles, S. W.; Morup, S. On Spin-Canting in Maghemite Particles. *J. Appl. Phys.* **1994**, *75*, 6583–6585.
29. Wang, B.; He, X.; Zhang, Z.; Zhao, Y.; Feng, W. Metabolism of Nanomaterials *in Vivo*: Blood Circulation and Organ Clearance. *Acc. Chem. Res.* **2012**, 10.1021/ar2003336.
30. Stark, W. J. Nanoparticles in Biological Systems. *Angew. Chem., Int. Ed.* **2011**, *50*, 1242–1258.
31. Albanese, A.; Tang, P. S.; Chan, W. C. W. The Effect of Nanoparticle Size, Shape, and Surface Chemistry on Biological Systems. *Annu. Rev. Biomed. Eng.* **2012**, *14*, 1–16.
32. Minchin, R. Nanomedicine: Sizing Up Targets with Nanoparticles. *Nat. Nanotechnol.* **2008**, *3*, 12–13.
33. Lundqvist, M.; Stigler, J.; Elia, G.; Lynch, I.; Cedervall, T.; Dawson, K. A. Nanoparticle Size and Surface Properties Determine the Protein Corona with Possible Implications for Biological Impacts. *Proc. Natl. Acad. Sci.* **2008**, *105*, 14265–14270.
34. Petros, R. A.; DeSimone, J. M. Strategies in the Design of Nanoparticles for Therapeutic Applications. *Nat. Rev. Drug Discovery* **2010**, *9*, 615–627.
35. Walkey, C. D.; Olsen, J. B.; Guo, H.; Emili, A.; Chan, W. C. W. Nanoparticle Size and Surface Chemistry Determine Serum Protein Adsorption and Macrophage Uptake. *J. Am. Chem. Soc.* **2011**, *134*, 2139–2147.
36. Longmire, M.; Choyke, P. L.; Kobayashi, H. Clearance Properties of Nano-Sized Particles and Molecules as Imaging Agents: Considerations and Caveats. *Nanomedicine* **2008**, *3*, 703–717.
37. Alexis, F.; Pridgen, E.; Molnar, L. K.; Farokhzad, O. C. Factors Affecting the Clearance and Biodistribution of Polymeric Nanoparticles. *Mol. Pharmaceut.* **2008**, *5*, 505–515.
38. Lee, H.; Lee, E.; Kim, D. K.; Jang, N. K.; Jeong, Y. Y.; Jon, S. Antibiofouling Polymer-Coated Superparamagnetic Iron Oxide Nanoparticles as Potential Magnetic Resonance Contrast Agents for *in Vivo* Cancer Imaging. *J. Am. Chem. Soc.* **2006**, *128*, 7383–7389.
39. Wei, H.; Insin, N.; Lee, J.; Han, H.-S.; Cordero, J. M.; Liu, W. h.; Bawendi, M. G. Compact Zwitterion-Coated Iron Oxide Nanoparticles for Biological Applications. *Nano Lett.* **2012**, *12*, 22–25.
40. Choi, H. S.; Liu, W.; Liu, F.; Nasr, K.; Misra, P.; Bawendi, M. G.; Frangioni, J. V. Design Considerations for Tumour-Targeted Nanoparticles. *Nat. Nanotechnol.* **2010**, *5*, 42–47.
41. Choi, H. S.; Liu, W.; Misra, P.; Tanaka, E.; Zimmer, J. P.; Itty Ipe, B.; Bawendi, M. G.; Frangioni, J. V. Renal Clearance of Quantum Dots. *Nat. Biotechnol.* **2007**, *25*, 1165–1170.
42. Sun, S. H.; Zeng, H. Size-Controlled Synthesis of Magnetite Nanoparticles. *J. Am. Chem. Soc.* **2002**, *124*, 8204–8205.
43. Dixit, G.; Pal Singh, J.; Srivastava, R. C.; Agrawal, H. M. Magnetic Resonance Study of Ce and Gd Doped $NiFe_2O_4$ Nanoparticles. *J. Magn. Magn. Mater.* **2012**, *324*, 479–483.
44. Sun, S.; Zeng, H.; Robinson, D. B.; Raoux, S.; Rice, P. M.; Wang, S. X.; Li, G. Monodisperse MFe_2O_4 (M = Fe, Co, Mn) Nanoparticles. *J. Am. Chem. Soc.* **2003**, *126*, 273–279.
45. Zhou, Z. J.; Huang, D. T.; Bao, J. F.; Chen, Q. L.; Liu, G.; Chen, Z.; Chen, X. Y.; Gao, J. H. A Synergistically Enhanced T_1-T_2 Dual-Modal Contrast Agent. *Adv. Mater.* **2012**, *24*, 6223–6228.
46. Jun, Y.-w.; Huh, Y.-M.; Choi, J.-s.; Lee, J.-H.; Song, H.-T.; Kim, S.; Yoon, S.; Kim, K.-S.; Shin, J.-S.; Suh, J.-S.; *et al*. Nanoscale Size Effect of Magnetic Nanocrystals and Their Utilization for Cancer Diagnosis *via* Magnetic Resonance Imaging. *J. Am. Chem. Soc.* **2005**, *127*, 5732–5733.
47. Aggarwal, P.; Hall, J. B.; McLeland, C. B.; Dobrovolskaia, M. A.; McNeil, S. E. Nanoparticle Interaction with Plasma Proteins As It Relates to Particle Biodistribution, Biocompatibility and Therapeutic Efficacy. *Adv. Drug Delivery Rev.* **2009**, *61*, 428–437.
48. Blazer-Yost, B. L.; Banga, A.; Amos, A.; Chernoff, E.; Lai, X.; Li, C.; Mitra, S.; Witzmann, F. A. Effect of Carbon Nanoparticles on Renal Epithelial Cell Structure, Barrier Function, and Protein Expression. *Nanotoxicology* **2011**, *5*, 354–371.
49. Sereemaspun, A.; Rojanathanes, R.; Wiwanitkit, V. Effect of Gold Nanoparticle on Renal Cell: An Implication for Exposure Risk. *Renal Failure* **2008**, *30*, 323–325.

50. Huang, J.; Bu, L. H.; Xie, J.; Chen, K.; Cheng, Z.; Li, X. G.; Chen, X. Y. Effects of Nanoparticle Size on Cellular Uptake and Liver MRI with Polyvinylpyrrolidone-Coated Iron Oxide Nanoparticles. *ACS Nano* **2010**, *4*, 7151–7160.
51. Feng, Y.; Zong, Y.; Ke, T.; Jeong, E.-K.; Parker, D. L.; Lu, Z.-R. Pharmacokinetics, Biodistribution and Contrast Enhanced MR Blood Pool Imaging of Gd-DTPA Cystine Copolymers and Gd-DTPA Cystine Diethyl Ester Copolymers in a Rat Model. *Pharm. Res.* **2006**, *23*, 1736–1742.
52. Gao, J. H.; Chen, K.; Xie, R. G.; Xie, J.; Lee, S.; Cheng, Z.; Peng, X. G.; Chen, X. Y. Ultrasmall Near-Infrared Non-Cadmium Quantum Dots for *in Vivo* Tumor Imaging. *Small* **2010**, *6*, 256–261.
53. Ba-Ssalamah, A.; Uffmann, M.; Saini, S.; Bastati, N.; Herold, C.; Schima, W. Clinical Value of MRI Liver-Specific Contrast Agents: A Tailored Examination for a Confident Non-Invasive Diagnosis of Focal Liver Lesions. *Eur. Radiol.* **2009**, *19*, 342–357.
54. Gao, J. H.; Chen, K.; Luong, R.; Bouley, D. M.; Mao, H.; Qiao, T.; Gambhir, S. S.; Cheng, Z. A Novel Clinically Translatable Fluorescent Nanoparticle for Targeted Molecular Imaging of Tumors in Living Subjects. *Nano Lett.* **2012**, *12*, 281–286.
55. Sandiford, L.; Phinikaridou, A.; Protti, A.; Meszaros, L. K.; Cui, X.; Yan, Y.; Frodsham, G.; Williamson, P. A.; Gaddum, N.; Botnar, R. M.; *et al*. Bisphosphonate-Anchored PEGylation and Radiolabeling of Superparamagnetic Iron Oxide: Long-Circulating Nanoparticles for *in Vivo* Multimodal (T1MRI-SPECT) Imaging. *ACS Nano* **2013**, *7*, 500–512.